ASTEROSEISMOLOGY OF THE SOLAR ANALOGS 16 Cyg A AND B FROM *KEPLER* OBSERVATIONS

T. S. Metcalfe[1,2,3], W. J. Chaplin[3,4], T. Appourchaux[5], R. A. García[3,6,7], S. Basu[3,8], I. Brandão[9], O. L. Creevey[10],
S. Deheuvels[3,8], G. Doğan[1,3], P. Eggenberger[11], C. Karoff[12], A. Miglio[3,4], D. Stello[13], M. Yıldız[14], Z. Çelik[14],
H. M. Antia[15], O. Benomar[13], R. Howe[4], C. Régulo[16,17], D. Salabert[10], T. Stahn[18,19], T. R. Bedding[3,13], G. R. Davies[6,7],
Y. Elsworth[4], L. Gizon[18,19], S. Hekker[4,20], S. Mathur[1,3], B. Mosser[21], S. T. Bryson[22], M. D. Still[22],
J. Christensen-Dalsgaard[1,3,12], R. L. Gilliland[23], S. D. Kawaler[3,24], H. Kjeldsen[3,12], K. A. Ibrahim[25],
T. C. Klaus[25], and J. Li[26]

[1] High Altitude Observatory, NCAR, P.O. Box 3000, Boulder, CO 80307, USA
[2] Computational & Information Systems Laboratory, NCAR, P.O. Box 3000, Boulder, CO 80307, USA
[3] Kavli Institute for Theoretical Physics, Kohn Hall, University of California, Santa Barbara, CA 93106, USA
[4] School of Physics and Astronomy, University of Birmingham, Edgbaston, Birmingham B15 2TT, UK
[5] Institut d'Astrophysique Spatiale, Univ Paris-Sud, UMR8617, CNRS, Bâtiment 121, 91405 Orsay Cedex, France
[6] Laboratoire AIM, CEA/DSM-CNRS-Université Paris Diderot, 91191 Gif-sur-Yvette Cedex, France
[7] IRFU/SAp, Centre de Saclay, 91191 Gif-sur-Yvette Cedex, France
[8] Department of Astronomy, Yale University, P.O. Box 208101, New Have, CT 06520-8101, USA
[9] Centro de Astrofísica and Faculdade de Ciências, Universidade do Porto, Rua das Estrelas, 4150-762 Porto, Portugal
[10] Laboratoire Lagrange, UMR7293, Observatoire de la Côte d'Azur, Université de Nice Sophia-Antipolis, CNRS, BP 4229, 06304 Nice Cedex 4, France
[11] Observatoire de Genève, Université de Genève, 51 Ch. des Maillettes, CH-1290 Sauverny, Switzerland
[12] Department of Physics and Astronomy, Aarhus University, DK-8000 Aarhus C, Denmark
[13] Sydney Institute for Astronomy (SIfA), School of Physics, University of Sydney, NSW 2006, Australia
[14] Department of Astronomy and Space Sciences, Ege University, Bornova, 35100 Izmir, Turkey
[15] Tata Institute of Fundamental Research, Homi Bhabha Road, Mumbai 400005, India
[16] Instituto de Astrofísica de Canarias, 38205 La Laguna, Tenerife, Spain
[17] Dpto de Astrofísica, Universidad de La Laguna, 38206 La Laguna, Tenerife, Spain
[18] Max-Planck-Institut für Sonnensystemforschung, 37191 Katlenburg-Lindau, Germany
[19] Institut für Astrophysik, Georg-August-Universität Göttingen, 37077 Göttingen, Germany
[20] Astronomical Institute "Anton Pannekoek," University of Amsterdam, Science Park 904, 1098 HX Amsterdam, The Netherlands
[21] LESIA-Observatoire de Paris, CNRS, Université Pierre et Marie Curie, Université Denis Diderot, 92195 Meudon Cedex, France
[22] NASA Ames Research Center, Moffett Field, CA 94035, USA
[23] Center for Exoplanets and Habitable Worlds, The Pennsylvania State University, University Park, PA 16802, USA
[24] Department of Physics and Astronomy, Iowa State University, Ames, IA 50011, USA
[25] Orbital Sciences Corporation/NASA Ames Research Center, Moffett Field, CA 94035, USA
[26] SETI Institute/NASA Ames Research Center, Moffett Field, CA 94035, USA

ABSTRACT

The evolved solar-type stars 16 Cyg A and B have long been studied as solar analogs, yielding a glimpse into the future of our own Sun. The orbital period of the binary system is too long to provide meaningful dynamical constraints on the stellar properties, but asteroseismology can help because the stars are among the brightest in the *Kepler* field. We present an analysis of three months of nearly uninterrupted photometry of 16 Cyg A and B from the *Kepler* space telescope. We extract a total of 46 and 41 oscillation frequencies for the two components, respectively, including a clear detection of octupole ($l = 3$) modes in both stars. We derive the properties of each star independently using the Asteroseismic Modeling Portal, fitting the individual oscillation frequencies and other observational constraints simultaneously. We evaluate the systematic uncertainties from an ensemble of results generated by a variety of stellar evolution codes and fitting methods. The optimal models derived by fitting each component individually yield a common age ($t = 6.8 \pm 0.4$ Gyr) and initial composition ($Z_i = 0.024 \pm 0.002$, $Y_i = 0.25 \pm 0.01$) within the uncertainties, as expected for the components of a binary system, bolstering our confidence in the reliability of asteroseismic techniques. The longer data sets that will ultimately become available will allow future studies of differential rotation, convection zone depths, and long-term changes due to stellar activity cycles.

Key words: stars: fundamental parameters – stars: individual (HD 186408, HD 186427) – stars: interiors – stars: oscillations – stars: solar-type

Online-only material: color figure

1. INTRODUCTION

Observations of the Sun provide an extraordinarily detailed snapshot of stellar structure and dynamics for a single set of physical properties and at a particular evolutionary state in the life of a star. To generalize our understanding of stellar evolution, and to evaluate the degree to which the Sun is typical or peculiar, it is useful to examine other classes of stars. Cayrel de Strobel

(1996) defined several such classes, including: *solar twins* with fundamental physical properties very similar or identical to the Sun, *solar analogs* which are broadly comparable to the recent past and near future of the Sun, and *solar-like stars* including a wider range of F and G dwarfs and subgiants. Well-known solar twins such as 18 Sco (Bazot et al. 2011) provide some context for the Sun observed as a star, while solar analogs like κ^1 Cet, β Hyi, and α Cen A and B (Walker et al. 2007; Brandão

et al. 2011; Bedding et al. 2004; Kjeldsen et al. 2005) help calibrate stellar evolution for stars that are younger, older, and more or less massive than the Sun. Broader studies of solar-like stars probe the full range of relevant stellar properties and evolutionary states (e.g., Chaplin et al. 2011; Silva Aguirre et al. 2011).

The bright stars 16 Cyg A and B ($\equiv$ HD 186408 and 186427 $\equiv$ KIC 12069424 and 12069449; $V \sim 6$) have long been studied as solar analogs, with estimated ages near 6–8 Gyr (Wright et al. 2004; Valenti & Fischer 2005). Although they are members of a hierarchical triple system with a red dwarf companion that is 10 mag fainter (Turner et al. 2001; Patience et al. 2002), there are no dynamical constraints on the masses because the available data suggest an orbital period longer than 18,000 years (Hauser & Marcy 1999). After the discovery of a 1.5 Jupiter-mass exoplanet in an eccentric 800 day orbit around 16 Cyg B (Cochran et al. 1997), the system generated even more interest. Since then, both components have been monitored for magnetic activity, showing long-term variations around a mean chromospheric activity level well below that of the Sun at solar minimum (J. Hall 2009, private communication). So far, there have been no direct measurements of rotation, but gyrochronology suggests that the rotation periods should be near 30 days (Skumanich 1972). As two of the brightest stars in the *Kepler* field of view, 16 Cyg A and B can now be subjected to a long-term study that promises to yield more detailed information than is currently available for any star but the Sun.

In this Letter, we perform an asteroseismic analysis of the first three months of data on 16 Cyg A and B from the *Kepler* mission (Koch et al. 2010). Using the unprecedented observations, we model the two components independently and determine an identical age and initial composition, as expected for the members of a binary system. In Section 2, we describe the data analysis methods, and in Section 3 we present the asteroseismic modeling including an evaluation of both the statistical and systematic uncertainties. We conclude in Section 4 with a discussion of the results and the potential for future studies utilizing the longer data sets that will soon become available.

2. DATA ANALYSIS

The first full quarter of short-cadence observations (58.85 s sampling; Gilliland et al. 2010) of 16 Cyg A and B was obtained by *Kepler* between 2010 September and December (Q7). Both stars are significantly brighter than the photometric saturation limit. Saturated flux is conserved on *Kepler*, so no photometric precision is lost for saturated targets as long as the saturated pixels are included in the pixel aperture. Standard *Kepler* pixel apertures were not designed for such bright, saturated targets and in the case of 16 Cyg contain a prohibitively large number of unneeded pixels. Custom masks were therefore defined from Q3 full frame images to capture all of the flux using fewer pixels. The raw photometric light curves extracted from these masks (Jenkins et al. 2010) were then prepared for asteroseismic analysis in the manner described by García et al. (2011). Figure 1 shows the power spectra of both stars (16 Cyg A in the left panels and 16 Cyg B in the right panels).

The top panels include boxcar smoothed power spectra (in gray) over an extended range in frequency, showing not only the Gaussian-like power excess due to solar-like oscillations, but also contributions to the background power-spectral density attributable to granulation (dashed lines), stellar activity and/or larger scales of granulation (dot-dashed lines), and shot noise (dotted lines). The backgrounds were fit with a three-component model, comprising two Harvey-like power laws (Harvey 1985) to represent granulation and activity, and a flat component to represent the contribution of shot noise. The best-fitting sum of background components is shown as a solid black line in each panel. We note that the best-fitting timescales ($\tau_{\mathrm{gran,A}} = 257 \pm 6$ s, $\tau_{\mathrm{gran,B}} = 241 \pm 8$ s) and peak powers ($P_{\mathrm{gran,A}} = 3.01 \pm 0.08$ ppm$^2\,\mu$Hz^{-1}, $P_{\mathrm{gran,B}} = 2.41 \pm 0.07$ ppm$^2\,\mu$Hz^{-1}) of the granulation components are both slightly greater than the solar values estimated from Sun-as-a-star observations, and follow the scaling relations derived by Kjeldsen & Bedding (2011).

The bottom panels show very clear patterns of peaks due to solar-like oscillations of high radial order n. The quality of the oscillation spectra are exquisite, with each star showing more than 15 radial overtones including many octupole ($l = 3$) modes. The maximum peak height-to-background ratios are comparable to those observed in photometric Sun-as-a-star data—the shot noise level is so low in these *Kepler* data that the intrinsic stellar granulation noise dominates the background across the frequency ranges where the modes are observed.

Ten teams provided estimates of the frequencies of the observed modes, applying *peak-bagging* techniques developed for application to *CoRoT* (Appourchaux et al. 2008) and *Kepler* data (e.g., see Campante et al. 2011; Mathur et al. 2011). These techniques varied in the details of the optimizations performed—which included classical maximum-likelihood estimation (e.g., Fletcher et al. 2011) and Markov Chain Monte Carlo methods (e.g., Handberg & Campante 2011)—and in the number of free parameters and assumptions made for fits of Lorentzian-like models to mode peaks in the power spectra.

The results of the 10 teams were analyzed to produce final frequency sets for each star. First, we sought to identify objectively those modes for which a robust, well-determined frequency could be estimated. This involved two types of checks. In one, we identified a list of modes with good agreement between the best-fitting frequencies from various teams. This was achieved using a modified version of the procedure outlined in Campante et al. (2011) and Mathur et al. (2011). A so-called *minimal frequency set* of modes was produced, for which a majority of the teams' estimates were retained after applying Peirce's criterion (Peirce 1852; Gould 1855) for outlier rejection. A second set of checks involved visual inspection of the frequency-power spectra (and échelle diagrams of those spectra), combined with objective false alarm probability (e.g., Chaplin et al. 2002) and likelihood ratio tests (e.g., Appourchaux 2011).

With a list of robust modes in hand, one of the teams was then selected to re-fit these modes in both stars using a single Lorentzian profile per mode (i.e., no rotational splitting and the inclination angle fixed at 0°). This team was chosen as the one whose initial best-fitting frequencies showed the closest match to the frequencies of the minimal set. Use of frequencies from one of the teams, as opposed to some average over all teams, meant that the modeling could rely on an easily reproducible set of input frequencies (see Table 1).

3. ASTEROSEISMIC MODELING

The set of oscillation modes from the peak-bagging analysis described in Section 2 included a total of 46 and 41 individual frequencies for 16 Cyg A and B, respectively. As inputs for
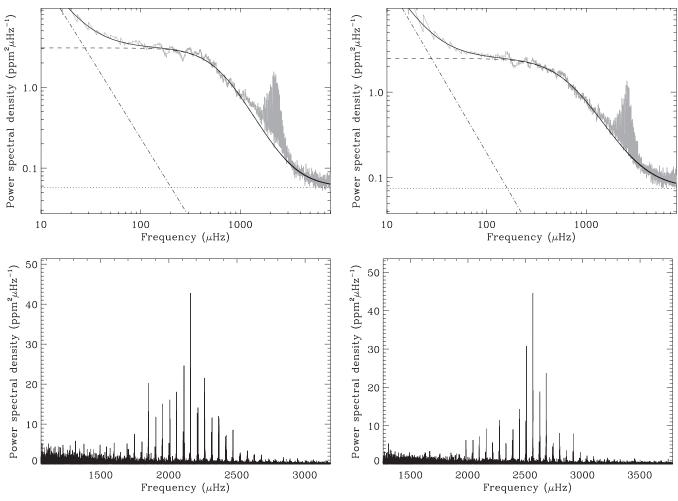
Figure 1. Power spectra of 16 Cyg A (left panels) and 16 Cyg B (right panels). Top panels: 20 μHz boxcar smoothed spectra (gray), with best-fitting background components attributed to granulation (dashed lines), stellar activity and/or larger scales of granulation (dot-dashed lines), and shot noise (dotted lines), with the sum of the background components plotted as solid black lines. Bottom panels: background-subtracted power spectra over the ranges in frequency where high-order p modes are observed.

Table 1
Observed Oscillation Frequencies for 16 Cyg A and B

n[a]	16 Cyg A				16 Cyg B			
	$\ell = 0$ (μHz)	$\ell = 1$ (μHz)	$\ell = 2$ (μHz)	$\ell = 3$ (μHz)	$\ell = 0$ (μHz)	$\ell = 1$ (μHz)	$\ell = 2$ (μHz)	$\ell = 3$ (μHz)
13	$\cdots$	$\cdots$	1591.21 ± 0.86	$\cdots$	$\cdots$	$\cdots$	$\cdots$	$\cdots$
14	1598.51 ± 0.27	1644.24 ± 0.33	1693.73 ± 0.46	1736.03 ± 1.84	$\cdots$	$\cdots$	1920.99 ± 0.24	$\cdots$
15	1700.43 ± 0.34	1746.93 ± 0.24	1795.87 ± 0.40	1839.07 ± 1.64	1928.81 ± 0.28	1982.66 ± 0.16	2036.59 ± 0.20	$\cdots$
16	1802.15 ± 0.17	1849.11 ± 0.13	1898.08 ± 0.27	1944.07 ± 1.57	2044.21 ± 0.15	2098.20 ± 0.17	2152.91 ± 0.19	2202.75 ± 0.65
17	1904.62 ± 0.15	1951.98 ± 0.16	2001.82 ± 0.17	2045.09 ± 0.80	2159.36 ± 0.16	2214.00 ± 0.18	2269.07 ± 0.21	2317.08 ± 0.44
18	2007.45 ± 0.13	2055.41 ± 0.16	2105.60 ± 0.15	2150.15 ± 0.19	2276.03 ± 0.12	2330.88 ± 0.16	2386.30 ± 0.17	2436.78 ± 0.33
19	2110.94 ± 0.11	2158.89 ± 0.12	2208.90 ± 0.19	2253.41 ± 0.35	2392.87 ± 0.14	2448.17 ± 0.11	2503.56 ± 0.13	2553.00 ± 0.23
20	2214.33 ± 0.17	2262.32 ± 0.16	2312.49 ± 0.29	2356.92 ± 0.46	2509.75 ± 0.13	2565.35 ± 0.10	2619.99 ± 0.23	2672.34 ± 0.28
21	2317.18 ± 0.17	2366.15 ± 0.16	2416.24 ± 0.33	2461.26 ± 1.04	2626.43 ± 0.11	2682.38 ± 0.14	2737.44 ± 0.31	2788.74 ± 1.40
22	2420.75 ± 0.30	2470.23 ± 0.25	2520.91 ± 0.81	$\cdots$	2743.15 ± 0.25	2799.67 ± 0.22	2854.52 ± 0.39	2906.96 ± 0.93
23	2524.94 ± 0.39	2575.97 ± 0.31	2624.05 ± 0.51	$\cdots$	2860.63 ± 0.26	2917.75 ± 0.22	2972.73 ± 0.70	$\cdots$
24	2629.36 ± 0.36	2678.47 ± 0.47	2730.06 ± 1.03	$\cdots$	2978.95 ± 0.40	$\cdots$	3089.46 ± 0.87	$\cdots$
25	2736.22 ± 1.45	2783.71 ± 1.22	$\cdots$	$\cdots$	3096.00 ± 0.54	3152.45 ± 0.61	$\cdots$	$\cdots$
26	2838.68 ± 0.38	2889.61 ± 0.38	$\cdots$	$\cdots$	3215.94 ± 0.91	3274.63 ± 0.55	$\cdots$	$\cdots$

Note. [a] Radial order n from the optimal AMP models.

the stellar modeling, we supplemented these asteroseismic constraints with the spectroscopic properties of each component derived by Ramírez et al. (2009) ($T_{\rm eff,A} = 5825 \pm 50$ K, $\log g_A = $ 4.33 $\pm$ 0.07, [Fe/H]$_A = 0.096 \pm 0.026$; $T_{\rm eff,B} = 5750 \pm 50$ K, $\log g_B = 4.34 \pm 0.07$, [Fe/H]$_B = 0.052 \pm 0.021$). Using these $T_{\rm eff}$ values to obtain bolometric corrections from Flower (1996)
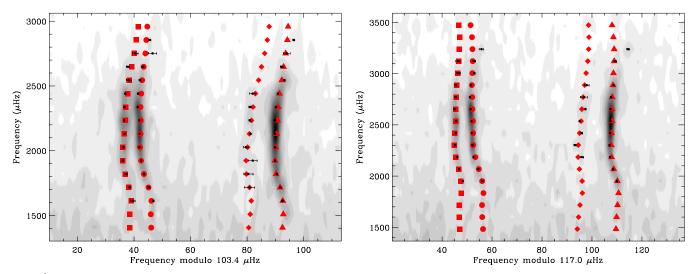
Figure 2. Échelle diagrams of 16 Cyg A (left) and 16 Cyg B (right), showing the observed frequencies as black points with horizontal error bars. The frequencies of the optimal models from AMP are shown using different red symbols to indicate modes with radial ($l = 0$, circles), dipole ($l = 1$, triangles), quadrupole ($l = 2$, squares), and octupole ($l = 3$, diamonds) geometries. A gray-scale map showing a Gaussian smoothed power spectrum (FWHM $\sim 2\ \mu$Hz) is included in the background for reference.

(A color version of this figure is available in the online journal.)

Table 2
Stellar Model-fitting Results for 16 Cyg A and B

	16 Cyg A							16 Cyg B						
	$R/R_\odot$	$M/M_\odot$	t (Gyr)	Z_i	Y_i	α	χ^2	$R/R_\odot$	$M/M_\odot$	t (Gyr)	Z_i	Y_i	α	χ^2
AMP	1.236	1.10	6.5	0.022	0.25	2.06	5.47	1.123	1.06	5.8	0.020	0.25	2.05	9.80
σ_{stat}	0.016	0.01	0.2	0.002	0.01	0.03	. . .	0.020	0.01	0.1	0.001	0.01	0.03	. . .
ANKİ	1.260	1.14	6.4	0.024	0.26	1.94	21.41	1.138	1.08	6.4	0.022	0.26	1.94	23.29
ASTEC1	1.237	1.10	7.5	0.023	0.25	2.00	5.70	1.121	1.05	7.3	0.021	0.25	2.00	7.97
ASTEC2	1.235	1.10	6.8	0.022	0.25	2.00	7.70	1.134	1.09	6.3	0.025	0.25	2.00	8.47
CESAM	1.253	1.14	7.0	0.027	0.24[a]	0.72[b]	3.53	1.136	1.09	6.9	0.025	0.24[a]	0.73[b]	4.78
Geneva	1.236	1.10	6.7[c]	0.024[c]	0.26[c]	1.80[c]	10.82	1.122	1.06	6.7[c]	0.024[c]	0.26[c]	1.80[c]	10.98
YREC	1.244	1.11	6.9	0.026	0.26	2.08	5.68	1.121	1.05	6.9[d]	0.022	0.26	1.84	3.17
Adopted	**1.243**	**1.11**	**6.9**	**0.024**	**0.25**	**2.00**	. . .	**1.127**	**1.07**	**6.7**	**0.023**	**0.25**	**1.92**	. . .
σ_{sys}	0.008	0.02	0.3	0.002	0.01	0.08	. . .	0.007	0.02	0.4	0.002	0.01	0.09	. . .

Notes.
[a] Values of $Y_i < 0.24$ excluded from search.
[b] Value of α from the Canuto et al. (1996) treatment of convection, excluded from average.
[c] Age, composition, and mixing-length constrained to be identical in both components.
[d] Age of 16 Cyg B constrained to be identical to the value found for 16 Cyg A.

and adopting $M_{\text{bol}} = 4.73 \pm 0.03$ from Torres (2010), we combined the extinction estimates from Ammons et al. (2006) with the updated *Hipparcos* parallaxes (van Leeuwen 2007) to derive luminosity constraints: $L_A = 1.56 \pm 0.05\ L_\odot$ and $L_B = 1.27 \pm 0.04\ L_\odot$.

We calculated separate values of χ^2 for the asteroseismic and spectroscopic constraints and attempted to minimize them simultaneously using the Asteroseismic Modeling Portal (AMP; Metcalfe et al. 2009). This automated method uses a parallel genetic algorithm to search a broad range of stellar parameters and objectively determines the globally optimal model for a given set of observations. Although 16 Cyg A and B are members of a binary system and presumably formed simultaneously from the same material, we fit each set of constraints independently and did not force the models to have a common age or initial composition. The oscillation frequencies of the optimal models for each star are plotted as red symbols in

Figure 2, where the observed modes are shown as black points with horizontal error bars. In both cases, the asteroseismic χ^2 is less than 10 and the spectroscopic χ^2 is less than 1, so the models represent a reasonably good match to both sets of observational constraints. In Table 2 we list the optimal values for the radius (R) and for the adjustable model parameters, including the mass (M), age (t), initial metallicity (Z_i) and helium mass fraction (Y_i), and the mixing-length parameter (α), along with the asteroseismic χ^2. The statistical uncertainties on each parameter (σ_{stat}) were determined using Singular Value Decomposition.

To evaluate the possible sources of systematic uncertainty from the ingredients and assumptions in our models, six teams were given the results from AMP and asked to reproduce the fit using the same set of observational constraints with their own stellar evolution codes and fitting methods. The physical ingredients adopted by each team differed slightly from those

employed by AMP,[27] allowing us to explore the degree of model dependence in our results. The optimal parameter values from each team are listed in Table 2, where we combine all of them into an adopted value (bold row) representing the average of the individual estimates weighted by $1/\chi^2$. The systematic uncertainty ($\sigma_{\rm sys}$) on each parameter reflects the variance of the results, again weighted by $1/\chi^2$.

As expected, there are slight differences between the optimal parameter values determined by each team. Since we effectively used AMP to solve the global optimization problem, these differences reflect subtle shifts in the locally optimal solution due to the physical ingredients included in each stellar evolution code. However, the results from different teams also include small offsets due to incomplete optimization—refined sampling of each adjustable parameter will always improve the fit, and there was no uniform criterion for when to stop fine tuning. To minimize the influence of this *technique error* on the final results, we weight the average parameter values and uncertainties using $1/\chi^2$ from each result as a proxy for the overall quality of the fit. This ensures that the variance reflects the actual systematic differences between model physics rather than the effort expended by each team in trying to match the observations. As with AMP, most of the teams did not force any of the model parameters of 16 Cyg A and B to share a common value. The exceptions were the Geneva code (which forced a common age, initial composition, and mixing length) and YREC (which forced the model for B to have the same age as the optimal model for A). Excluding these models from the average does not significantly change the values of the adopted parameters listed in Table 2.

4. RESULTS AND DISCUSSION

We have performed an analysis of the solar analogs 16 Cyg A and B using 3 months of observations from the *Kepler* space telescope, yielding the highest quality asteroseismic data sets for any star but the Sun (see Figure 1). We identify a total of 46 and 41 oscillation frequencies in the two components, respectively, including a clear detection of octupole ($l = 3$) modes in both stars. These modes are difficult to detect in photometric data because the bright and dark patches associated with higher degree modes are normally expected to cancel in disk-integrated measurements. The unambiguous detection of such modes from the *Kepler* light curves of 16 Cyg A and B is a testament to the exceptional quality of the data.

We derived the properties of each star independently by fitting stellar models to the oscillation frequencies (see Table 1) and other observational constraints (see Section 3) simultaneously. The initial results from fitting each star individually using

the AMP (see Figure 2) yield the same initial composition within the statistical uncertainties and a similar age for the two components. Further analysis using several stellar evolution codes employing a variety of input physics allows us to quantify the model dependence of our results, and to adopt reliable values and uncertainties from the ensemble. The adopted stellar properties of 16 Cyg A and B (see Table 2) reinforce the conclusion that the two stars share a common age ($t = 6.8 \pm 0.4$ Gyr) and initial composition ($Z_{\rm i} = 0.024 \pm 0.002$ and $Y_{\rm i} = 0.25 \pm 0.01$), as expected for a binary system but without imposing this as a constraint for the modeling. This fundamental result bolsters our confidence in the reliability of asteroseismic inferences of stellar structure and evolution.

The relative size of the statistical and systematic uncertainties provides an important benchmark for what we can expect from asteroseismology with the *Kepler* mission. The statistical uncertainties on the stellar radii from AMP were derived from the distribution of radii in an ensemble of models that differ from the optimal model by $\pm 1\sigma$ for each adjustable parameter. Such estimates implicitly include the influence of parameter correlations and are consequently much larger than the systematic variation in optimal radii from different stellar evolution codes. This is not the case for adjustable model parameters like the mass and age, where $\sigma_{\rm sys}$ can be 2–4 times larger than $\sigma_{\rm stat}$, while the two are roughly comparable for the initial metallicity and helium mass fraction. The mixing-length parameter is a special case, because the range of estimates from different stellar evolution codes reflect variations in the solar-calibrated values that arise from differences in the input physics and in the specific formulation of mixing-length theory that is implemented in each code. Thus, the systematic uncertainties on α are likely to be overestimated, and small variations in the optimal value of this parameter from different codes should not be overinterpreted.

These extraordinary results were possible using just the first 3 months of short-cadence observations (Q7) from *Kepler*. Nine months of data will soon be available (Q7–8–9), and the stars continue to be on the short-cadence target list—at least through Q12 and hopefully for the remainder of the mission. These longer data sets will gradually yield higher frequency precision and improve the signal-to-noise ratio in the power spectra, enabling further characterization of the stars from the current frequency sets and facilitating detection of additional oscillation modes at higher and lower frequencies.

From 6–9 months of data we may begin to resolve rotational splitting of the non-radial oscillation modes into multiple components with different azimuthal orders, m. The variation of this splitting as a function of the radial order n can probe radial differential rotation, while the differences between non-radial modes with different spherical degrees l can reveal latitudinal variations. Such measurements of rotation may help to constrain possible scenarios to explain the different Li abundances of the two stars (Schuler et al. 2011; Ramírez et al. 2011). With 12–18 months of data, the frequency precision may be sufficient to resolve oscillatory signals in the deviations from uniform frequency spacing (so-called second differences, $\delta_2 \nu$) which reflect the acoustic depths of sharp transitions in the stellar structure, such as the helium ionization region and the base of the surface convection zone. Even longer data sets will allow us to probe the influence of stellar activity cycles, which lead to small anti-correlated changes in the frequencies and amplitudes of the oscillation modes. By the end of the baseline *Kepler* mission, and hopefully through an extended mission, these two

---

[27] AMP uses the OPAL 2005 equation of state and the most recent OPAL opacities supplemented by Alexander & Ferguson (1994) opacities at low temperature, nuclear reaction rates from Bahcall & Pinsonneault (1992), and includes the effects of helium diffusion and settling following Michaud & Proffitt (1993). Convection is treated with standard mixing-length theory without overshooting (Böhm-Vitense 1958). ANKİ solves the Saha equation itself, uses low temperature opacities from Ferguson et al. (2005), nuclear reaction rates primarily from Caughlan & Fowler (1988), and includes a full treatment of diffusion following Thoul et al. (1994). ASTEC1 and ASTEC2 use Ferguson et al. (2005) opacities, NACRE reaction rates (Angulo et al. 1999), and neglect diffusion. CESAM uses NACRE reaction rates and treats convection following Canuto et al. (1996). Geneva uses NACRE reaction rates and treats diffusion following Paquette et al. (1986). YREC uses Ferguson et al. (2005) opacities, nuclear reaction rates primarily from Adelberger et al. (1998), treats diffusion following Thoul et al. (1994), and includes convective overshooting. All models include the empirical correction for surface effects proposed by Kjeldsen et al. (2008).

bright solar analogs promise to yield the clearest picture yet of the future of our own Sun.

REFERENCES

Adelberger, E. G., Austin, S. M., Bahcall, J. N., et al. 1998, Rev. Mod. Phys., 70, 1265
Alexander, D. R., & Ferguson, J. W. 1994, ApJ, 437, 879
Ammons, S. M., Robinson, S. E., Strader, J., et al. 2006, ApJ, 638, 1004
Angulo, C., Arnould, M., Rayet, M., et al. 1999, Nucl. Phys. A, 656, 3
Appourchaux, T. 2011, Canary Islands Winter School of Astrophysics (Cambridge: Cambridge Univ. Press), in press (arXiv:1103.5352)
Appourchaux, T., Michel, E., Auvergne, M., et al. 2008, A&A, 488, 705
Bahcall, J. N., & Pinsonneault, M. H. 1992, Rev. Mod. Phys., 64, 885
Bazot, M., Ireland, M. J., Huber, D., et al. 2011, A&A, 526, L4
Bedding, T. R., Kjeldsen, H., Butler, R. P., et al. 2004, ApJ, 614, 380
Böhm-Vitense, E. 1958, Z. Astrophys., 46, 108
Brandão, I. M., Doğan, G., Christensen-Dalsgaard, J., et al. 2011, A&A, 527, A37
Campante, T. L., Handberg, R., Mathur, S., et al. 2011, A&A, 534, A6
Canuto, V. M., Goldman, I., & Mazzitelli, I. 1996, ApJ, 473, 550
Caughlan, G. R., & Fowler, W. A. 1988, At. Data Nucl. Data Tables, 40, 283
Cayrel de Strobel, G. 1996, A&AR, 7, 243

Chaplin, W. J., Elsworth, Y., Isaak, G. R., et al. 2002, MNRAS, 336, 979
Chaplin, W. J., Kjeldsen, H., Christensen-Dalsgaard, J., et al. 2011, Science, 332, 213
Cochran, W. D., Hatzes, A. P., Butler, R. P., & Marcy, G. W. 1997, ApJ, 483, 457
Ferguson, J. W., Alexander, D. R., Allard, F., et al. 2005, ApJ, 623, 585
Fletcher, S. T., Broomhall, A.-M., Chaplin, W. J., et al. 2011, MNRAS, 413, 359
Flower, P. J. 1996, ApJ, 469, 355
García, R. A., Hekker, S., Stello, D., et al. 2011, MNRAS, 414, L6
Gilliland, R. L., Jenkins, J. M., Borucki, W. J., et al. 2010, ApJ, 713, L160
Gould, B. A. 1855, AJ, 4, 81
Handberg, R., & Campante, T. L. 2011, A&A, 527, A56
Harvey, J. 1985, in Future Missions in Solar, Heliospheric & Space Plasma Physics, ed. E. Rolfe & B. Battrick (ESA SP-235; Noordwijk: ESA), 199
Hauser, H. M., & Marcy, G. W. 1999, PASP, 111, 321
Jenkins, J. M., Caldwell, D. A., Chandrasekaran, H., et al. 2010, ApJ, 713, L87
Kjeldsen, H., & Bedding, T. R. 2011, A&A, 529, L8
Kjeldsen, H., Bedding, T. R., Butler, R. P., et al. 2005, ApJ, 635, 1281
Kjeldsen, H., Bedding, T. R., & Christensen-Dalsgaard, J. 2008, ApJ, 683, L175
Koch, D. G., Borucki, W. J., Basri, G., et al. 2010, ApJ, 713, L79
Mathur, S., Handberg, R., Campante, T. L., et al. 2011, ApJ, 733, 95
Metcalfe, T. S., Creevey, O. L., & Christensen-Dalsgaard, J. 2009, ApJ, 699, 373
Michaud, G., & Proffitt, C. R. 1993, in ASP Conf. Ser. 40, Proc. IAU Colloq. 137: Inside the Stars, ed. A. Baglin & W. W. Weiss (San Francisco, CA: ASP), 246
Paquette, C., Pelletier, C., Fontaine, G., & Michaud, G. 1986, ApJS, 61, 177
Patience, J., White, R. J., Ghez, A. M., et al. 2002, ApJ, 581, 654
Peirce, B. 1852, AJ, 2, 161
Ramírez, I., Meléndez, J., & Asplund, M. 2009, A&A, 508, L17
Ramírez, I., Meléndez, J., Cornejo, D., Roederer, I. U., & Fish, J. R. 2011, ApJ, 740, 76
Schuler, S. C., Cunha, K., Smith, V. V., et al. 2011, ApJ, 737, L32
Silva Aguirre, V., Chaplin, W. J., Ballot, J., et al. 2011, ApJ, 740, L2
Skumanich, A. 1972, ApJ, 171, 565
Thoul, A. A., Bahcall, J. N., & Loeb, A. 1994, ApJ, 421, 828
Torres, G. 2010, AJ, 140, 1158
Turner, N. H., ten Brummelaar, T. A., McAlister, H. A., et al. 2001, AJ, 121, 3254
Valenti, J. A., & Fischer, D. A. 2005, ApJS, 159, 141
van Leeuwen, F. 2007, A&A, 474, 653
Walker, G. A. H., Croll, B., Kuschnig, R., et al. 2007, ApJ, 659, 1611
Wright, J. T., Marcy, G. W., Butler, R. P., & Vogt, S. S. 2004, ApJS, 152, 261